Visible light-assisted NGO-Fe_3O_4 composite activated peroxydisulfate for degradation of oxytetracycline

Jing Bai, Junfeng Wu, Zhi Li, Zhaodong Wang, Zuwen Liu, Biao Liu, Yanli Mao, Yifei Guo and Xianli Wang

ABSTRACT

A nitrogen-doped reduced graphene oxide/Fe_3O_4 composite (NGO-Fe_3O_4) was prepared through the simplified hydrothermal and deposition-precipitation method and characterized by X-ray diffraction, scanning electron microscopy and Fourier transform infrared spectroscopy. The degradation efficiency of oxytetracycline (OTC) by NGO-Fe_3O_4 activated peroxodisulfate (PDS) under visible light irradiation was studied. The degradation efficiency reached 100% within 32.5 min (the initial OTC concentration 50 mg L^{-1} and PDS 1 mM; [NGO-Fe_3O_4]:[PDS] = 4:1; pH = 3.0). No apparent decrease in degradation efficiency was observed after five cycles. $SO_4^{\cdot-}$ and ·OH were the main active oxides for OTC degradation in this system. Moreover, four degradation pathways were proposed, namely hydroxylation, dehydration, decarbonylation and demethylation according to the analysis results of high-performance liquid chromatography mass spectrometry.

Key words | NGO-Fe_3O_4, oxytetracycline, peroxydisulfate

Jing Bai
Zuwen Liu
School of Architectural and Surveying & Mapping Engineering,
Jiangxi University of Science and Technology,
Ganzhou 341000,
China

Jing Bai
Junfeng Wu (corresponding author)
Zhi Li
Zhaodong Wang
Biao Liu
Yanli Mao
Yifei Guo
Xianli Wang
Henan Province Key Laboratory of Water Pollution Control and Rehabilitation Technology,
Henan University of Urban Construction,
Pingdingshan, 467036,
China
E-mail: *wjf8047@163.com*

INTRODUCTION

Oxytetracycline (OTC) has been widely used in the treatment and prevention of human diseases (Watkinson *et al.* 2009). Trace antibiotics in the environment interfere with the development of ecosystems and human health by generating drug resistance, which has caused widespread concern. OTC is not readily biodegradable and difficult to be degraded by traditional biological treatment processes due to its hydrophilic and stable tetracene ring structure (Watkinson *et al.* 2007). OTC can cause water pollution through biological enrichment, so research on effective treatment techniques for removing these antibiotics is very important.

In order to control the sustained release and accumulation of antibiotics, it is necessary to improve the status quo through efficient degradation techniques, such as membrane filtration (Sharma *et al.* 2017; Wang *et al.* 2017), activated carbon adsorption (Huang *et al.* 2014; Zhu *et al.* 2014) and advanced oxidation processes (AOPs) (Oturan *et al.* 2013; Luu & Lee 2014). Since adsorption treatment hardly decomposes pollutants, which require proper subsequent treatment, more research methods for destructive degradation of OTC need to be explored. AOPs are generally regarded as excellent alternatives, especially for the degradation of emerging pollutants in the environment. AOPs based on $SO_4^{\cdot-}$ are a potential *in situ* chemical oxidation technology, and are widely used for remediation of groundwater and soil due to the strong oxidation capacity, long half-life (half period = 4 s) (Shiraz *et al.* 2017) and high free radical stability of $SO_4^{\cdot-}$. Common methods for producing $SO_4^{\cdot-}$ by activated persulfate (PDS) or peronosulfate include the use of ultraviolet (Bi *et al.* 2016), ultrasonic (Chen & Zheng 2015), heat (Olmezhanci *et al.* 2013), organic matter (Pu *et al.* 2017), carbon materials (Duan *et al.* 2017) and homogeneous transition metals or heterogeneous forms (Xiong *et al.* 2014). Heterogeneous activation is superior to homogeneous activation due to its mild reaction conditions and low risk of secondary pollution. In addition, magnetite (Fe_3O_4) is a heterogeneous catalyst that can exist stably at ambient temperature, and can be reused through magnetic separation to achieve cost savings (Ding *et al.* 2017). However, Fe_3O_4 particles tend to agglomerate into large particles leading to a decrease in dispersibility and catalytic activity (Peng *et al.* 2018; Zhu 2019). Moreover, graphene oxide (GO) has a unique two-dimensional layer structure of sp^2-bonded carbon atoms (Zhen *et al.* 2014),

doi: 10.2166/wst.2020.164

showing the advantage of a huge specific surface area. Therefore, The GO can serve as a carrier to prevent aggregation of the transition metal oxide. Some research results have shown doping the carbon network of reduced graphene oxide (RGO) with N atoms can introduce catalytic active sites (Wang *et al.* 2015). There is no influence on the lattice of the carbon material since the N atoms and the C atoms are adjacent in the periodic table and the atomic radii are similar. Moreover, a lone pair of electrons formed by doping N atoms can increase the charge density of the carbon material and correspondingly enhance its electron transfer ability and chemical activity (Xinran *et al.* 2009). In this study, a N-doped reduced graphene oxide/Fe_3O_4 composite (NGO-Fe_3O_4) was successfully synthesized by a hydrothermal and coprecipitation method. The visible-light (VIS)/NGO-Fe_3O_4/PDS process can effectively overcome the problems existing in the current use of such catalysts, improve the catalytic activity, and quickly and effectively remove antibiotic pollutants in wastewater. In addition, the catalyst can be recycled and costs reduced through magnetic recovery (Peng *et al.* 2018). Further research on its influencing factors, catalytic reaction mechanism, degradation kinetics and degradation pathways will provide technical support for the advanced treatment of bio-refractory wastewater in the actual production process. The main objectives were to: (a) study the effect of OTC degradation by Vis/NGO-Fe_3O_4/PDS process and optimization; (b) analyze the catalytic mechanism and main active substances of NGO-Fe_3O_4 on PDS; (c) explore the OTC degradation intermediates and degradation pathways.

EXPERIMENTAL

Reagents

Oxytetracycline ($C_{22}H_{28}N_2O_{11}$, 98.0%) was purchased from Huamaike Biotechnology Co., Ltd (Beijing, China). Graphite powder (C), ferrous sulfate ($FeSO_4{\cdot}7H_2O$, 99.0%) and potassium persulfate ($K_2S_2O_8$) were supplied by Sinopharm Chemical Reagent Co., Ltd (Shanghai, China). Hydrochloric acid (36–38%), sulfuric acid (95–98%), phosphate (≥85%), ammonia (25–28%), acetonitrile (CH_3CN) and methanol (CH_3OH) were obtained from Sinopharm Chemical Reagent Co., Ltd (Shanghai, China). Other reagents used in this study were provided by Luoyang Chemical Reagent Factory. All chemicals were of analytical grade or higher. Ultra-pure water was employed throughout the experiments.

Preparation of NGO-Fe_3O_4

GO was synthesized by a modified Hummers method. After ultrasonication for 30 min, 3 mL of $NH_3{\cdot}H_2O$ (25–28%) was added, transferred to a high-pressure reaction vessel lined with polytetrafluoroethylene (PTFE), and then heated at 180 °C for 24 h. A suspension of N atom doped reduced graphene oxide (NGO) was obtained. The pH of the NGO suspension was adjusted to 11 with $NH_3{\cdot}H_2O$ (25–28%). Four millilitres of $FeSO_4{\cdot}7H_2O$ (0.35 mg L^{-1}) was added and quickly stirred for 2 min, then heated in a water bath at 85 °C for 6 h to obtain NGO-Fe_3O_4 suspension. NGO-Fe_3O_4 was washed with deionized water to neutral, and the precipitate was dried in a petri dish.

Experimental procedure

Batch trials were performed in glass bottles with OTC solution. Adsorption experiments were started by adding NGO-Fe_3O_4 into solution and the mixture was placed on a mechanical stirrer (350 r/min) for 15 min. After the adsorption–desorption equilibrium reached, PDS was added and irradiated with a xenon lamp (500 W/50 Hz). Samples were taken out at predetermined time intervals and filtered through a 0.22 μm PTFE syringe filter. Methanol was added to quench the reaction for the antibiotic determination by high-performance liquid chromatography mass spectrometry (LC-MS).

Characterization methods

The surface morphology was observed by a field emission scanning electron microscope (SEM, SU-8010, Hitachi, Japan) equipped with an energy-dispersive X-ray analyzer. The crystal structure was characterized by X-ray diffraction (XRD, Rigaku S2, Japan). The Fourier transform infrared (FTIR) spectrum was recorded by a GX spectrophotometer (Perkin Elmer, USA) with the KBr wafer technique.

RESULTS AND DISCUSSION

Characterization of NGO-Fe_3O_4

The SEM photographs of GO, NGO, Fe_3O_4 and NGO-Fe_3O_4 are shown in Figure 1. GO was an ultra-thin graphene layered deposit. Due to the reduction of oxygen-containing functional groups and the increase of surface defects after the hydrothermal reaction, NGOs show a clear and large

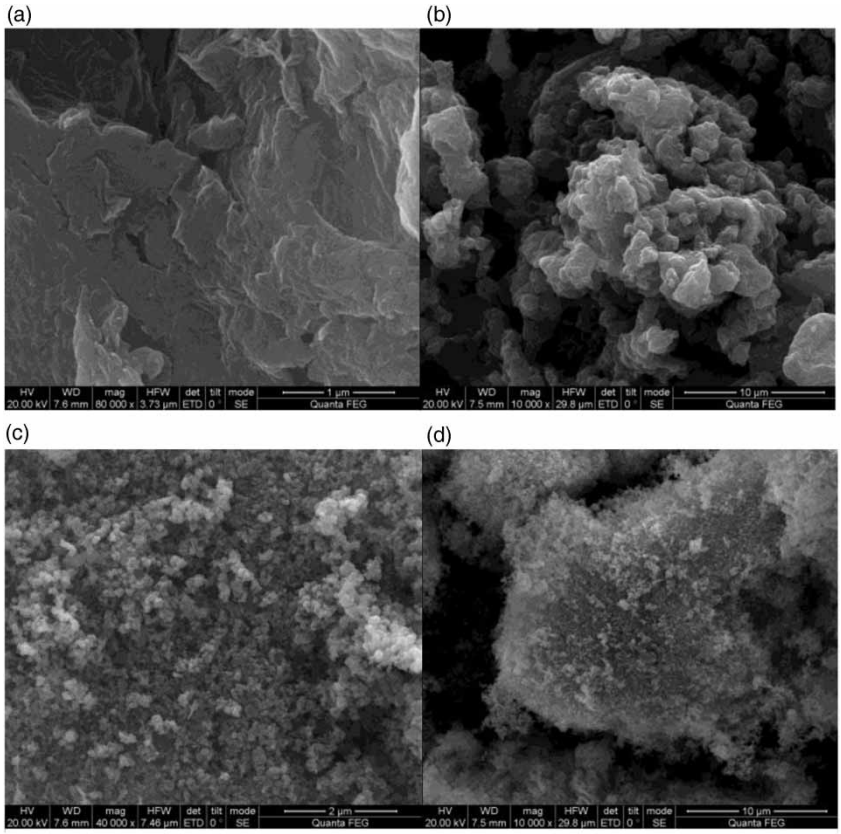

Figure 1 | SEM photographs of (a) GO, (b) NGO, (c) Fe_3O_4, (d) NGO-Fe_3O_4.

number of interconnected 3D porous structures in Figure 1(b). Fe_3O_4 was an irregular particle with a small particle size, in agglomerated or dispersed state. For NGO-Fe_3O_4, Fe_3O_4 particles were uniformly dispersed on the NGO porous structure, avoiding agglomeration of Fe_3O_4 particles and NGO materials.

In Figure 2, the functional groups of the NGO, Fe_3O_4 and NGO-Fe_3O_4 were identified by FTIR spectroscopy. The peak intensities of NGO relative to GO oxygen-containing groups decreased significantly, indicating that some oxygen-containing groups were eliminated after hydrothermal reaction (Donghui *et al.* 2010). In the FTIR spectrum of NGO, the representative peaks of 3,144.47, 1,626.47 and 1,052.94 cm^{-1} correspond to O–H stretching vibration of –OH group, C=O stretching vibration of -COOH group and C=O stretching vibration of -RO group, respectively (Peng *et al.* 2018). The representative peak of 1,223.53 cm^{-1} was attributed to the stretching vibration of C=N, indicating that amination function-modified GO material was formed by introducing a nitrogen-containing functional group (Lai *et al.* 2011).

Figure 3 shows the XRD patterns of GO, NGO, Fe_3O_4 and NGO-Fe_3O_4. The main broad diffraction peak of NGO appeared at 26.82° and 44.34°, while the characteristic peak of GO was 21.5°. In comparison with GO, the interlayer distance of NGO had become larger, indicating that the NGO sheet material had been effectively separated to a large extent. Moreover, the positions of the individual peaks of the NGO were similar as those of GO, revealing that the introducing N atom did not destroy the structure of GO (Liu *et al.* 2019). The diffraction peak at 26.8° of NGO supported by Fe_3O_4 disappeared, which was attributed to the fact that the crystal growth of Fe_3O_4 inhibited the restacking of GO layers, resulting in the decreasing of the crystal structure integrity of GO (Peng *et al.* 2018). In NGO-Fe_3O_4, the diffraction peaks at 30.06°, 35.38°, 43.06°, 53.50°, 56.98° and 62.70° can be attributed to the surface-centered cubic crystal plane of the Fe_3O_4 particles (Hu *et al.* 2012), and were almost the same as the Fe_3O_4 standard data (Christgau *et al.* 2004).

Catalytic activity comparison

As shown in Figure 4, the catalytic activity of NGO-Fe_3O_4 was evaluated by comparing the effects of different reaction processes on OTC degradation. The OTC degradation

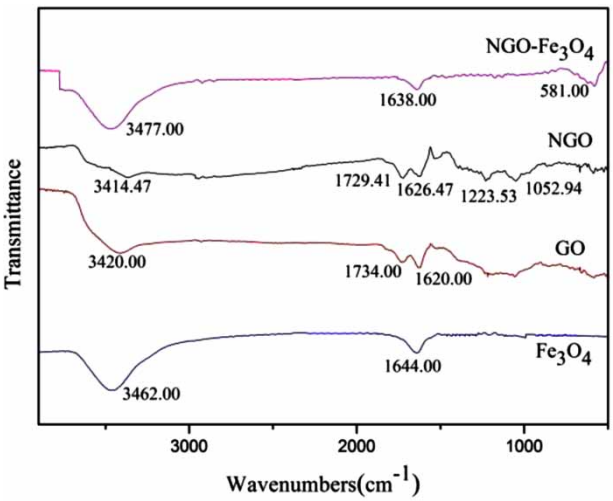

Figure 2 | FTIR spectra of of GO, NGO, Fe_3O_4 and NGO-Fe_3O_4.

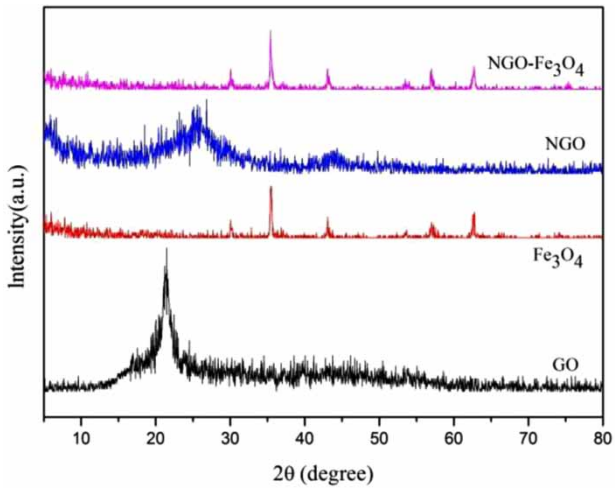

Figure 3 | XRD spectra of GO, NGO, Fe_3O_4 and NGO-Fe_3O_4.

efficiencies were only 19.05%, 35.18%, 37.18% and 31.5% by PDS, NGO-Fe_3O_4/PDS, Vis/NGO-Fe_3O_4 and Vis/PDS. However, the OTC degradation efficiency increased to 99.9% by Vis/NGO-Fe_3O_4/PDS systems. The OTC degradation by the Vis/NGO-Fe_3O_4/PDS system followed the first-order degradation kinetics (k_{obs}). The first-order degradation kinetic constant of Vis/NGO-Fe_3O_4/PDS (0.108 min^{-1}) was 36.0, 15.4, 10.8 and 13.5 times that of the PDS (0.003 min^{-1}), Vis/PDS (0.007 min^{-1}), Vis/NGO-Fe_3O_4 (0.010 min^{-1}), and NGO-Fe_3O_4/PDS (0.008 min^{-1}), respectively. It demonstrated a distinct synergistic effect was achieved in the Vis/NGO-Fe_3O_4/PDS system. This trend was mainly attributed to the rapid activation of PDS by Fe^{2+} in the initial reaction to produce a large amount of $SO_4^{-}\cdot$, and the reaction of $SO_4^{-}\cdot$ with contaminants, resulting in the sharp elimination of OTC. In the subsequent reaction, Fe^{2+} is gradually consumed to produce Fe^{3+}, which resulted in a slower degradation of the OTC observed in the subsequent time. However, since Fe^{3+} and OTC-Fe^{3+} can be converted into Fe^{2+} and OTC-Fe^{2+} under Vis irradiation (Equations (1)–(3)) (Bi *et al.* 2016), a stable catalytic activity can be maintained and a high OTC degradation efficiency can be achieved.

$$Fe^{2+} + S_2O_8^{2-} \rightarrow Fe^{3+} + SO_4^{2-} + SO_4^{-}\cdot \quad (1)$$

$$Fe^{3+} + Vis \rightarrow Fe^{2+} \quad (2)$$

$$OTC - Fe^{3+} + Vis \rightarrow OTC - Fe^{2+} \quad (3)$$

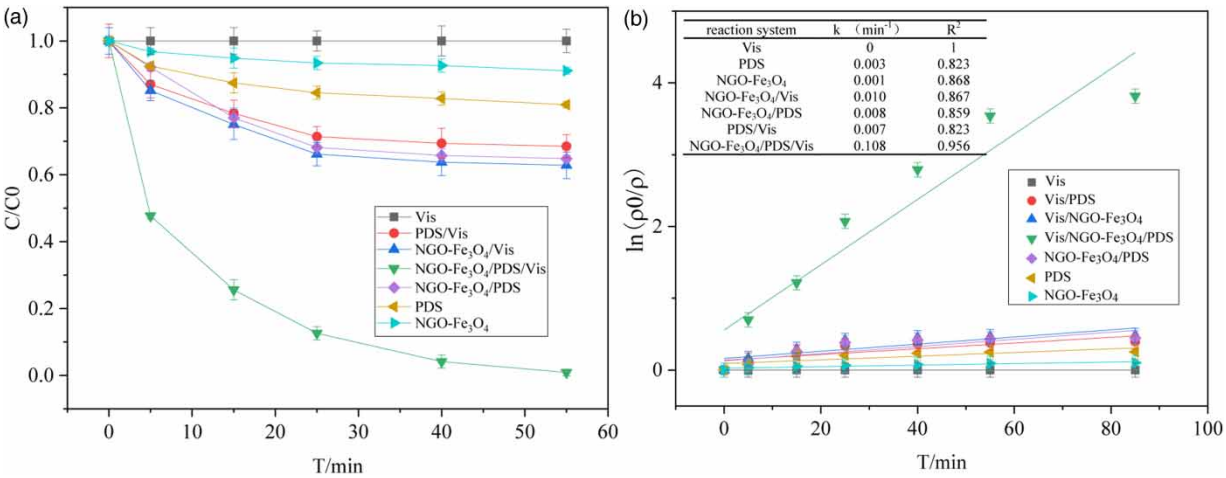

Figure 4 | (a) The degradation of oxytetracycline under different system conditions, and (b) degradation kinetics of oxytetracycline under different system conditions (initial OTC concentration = 50 mg L^{-1}, PDS concentration = 1 mM, NGO-Fe_3O_4 = 0.5 mg L^{-1}, temperature = 20 ± 2 °C, xenon lamp (500 W/50 Hz)).

Effects of different parameters on the catalytic activity of NGO-Fe_3O_4

Ratio of NGO-Fe_3O_4 to PDS

As shown in Figure 5, the effect of the ratio of NGO-Fe_3O_4 to PDS was explored for the OTC degradation by Vis/NGO-Fe_3O_4/PDS process. The results showed that the OTC degradation efficiencies were 46.4%, 66.9%, 81.3%, 92.2% and 100%, when the ratio of NGO-Fe_3O_4 to PDS was 1:4, 1:2, 1:1, 2:1 and 4:1, respectively. This trend was mainly due to the increase of the NGO-Fe_3O_4 dosage. Correspondingly, the active sites increased and then the OTC degradation efficiency increased. However, the k_{obs} decreased from 0.170 min^{-1} to 0.138 min^{-1} with the ratio of NGO-Fe_3O_4 and PDS increasing from 4:1 to 6:1. On the one hand, due to the reaction of the excess Fe^{2+} with $SO_4^{-}\cdot$ (Equation (4)), $SO_4^{-}\cdot$ was consumed and thus the OTC degradation efficiency decreased. On the other hand, excessive addition of NGO-Fe_3O_4 causes the suspended matter in the reaction solution to scatter light, so that the transmittance of light is reduced (Chen & Chu 2012), and the utilization of photons is reduced, thereby degrading the OTC degradation efficiency.

$$Fe^{2+} + SO_4^{-}\cdot \rightarrow Fe^{3+} + SO_4^{2-} \quad (4)$$

pH

Reaction pH was an important parameter for the OTC degradation by the Vis/NGO-Fe_3O_4/PDS system. First, the concentration and morphology of reactive free radicals depend on pH, and secondly, OTC has different pKa values under different pH conditions, showing different forms of existence (Figueroa *et al.* 2004). The effect of the Vis/NGO-Fe_3O_4/PDS process on OTC degradation efficiency under different pH conditions is shown in Figure 6. The degradation efficiency of OTC can reach more than 85% within 48 min, when the pH was 3.0, 4.0, 5.0, and 6.0. With the gradual decrease in pH, the k_{obs} gradually increased. Due to the positive zeta potential of NGO-Fe_3O_4 at pH 3.0–10.0, repulsive or attractive occurred between catalyst and antibiotic with equal or different charges (Pereira *et al.* 2011), respectively. Consequently, it was possible that the potential electrostatic repulsion was unfavorable for OTC molecular degradation. Under the conditions of pH 8.0 and 9.0, the degradation efficiency of OTC was only 52.01% and 49.53%, and the k_{obs} reduced to 0.007 min^{-1}. In alkaline environment, due to the increase of OH^- concentration, the reaction of $SO_4^{-}\cdot$ with OH^- gradually became significant (Equation (5)). This might lessen the contribution of $SO_4^{-}\cdot$ to the OTC removal. Moreover, ·OH could be scavenged by OH^- and SO_4^{-}, as shown in Equations (6) and (7) (Criquet & Leitner 2009).

$$SO_4^{-}\cdot + OH^- \rightarrow SO_4^{2-} + \cdot OH \quad (5)$$

$$\cdot OH + OH^- \rightarrow O^-\cdot + H_2O \quad (6)$$

$$SO_4^{-}\cdot + \cdot OH \rightarrow HSO_4^- + 0.5O_2 \quad (7)$$

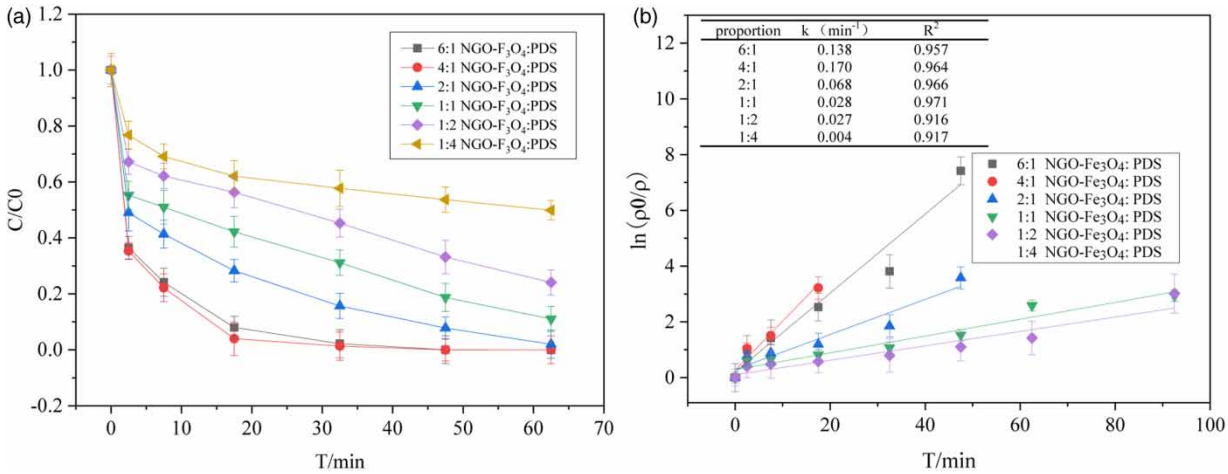

Figure 5 | (a) The degradation of oxytetracycline under different ratio conditions, and (b) degradation kinetics of oxytetracycline under different ratio conditions (initial OTC concentration = 50 mg L^{-1}, PDS concentration = 1 mM, [NGO-Fe_3O_4] : [PDS] = 6:1, 4:1, 2:1, 1:1, 1:2, 1:4, temperature = 20 ± 2 °C, xenon lamp (500 W/50 Hz)).

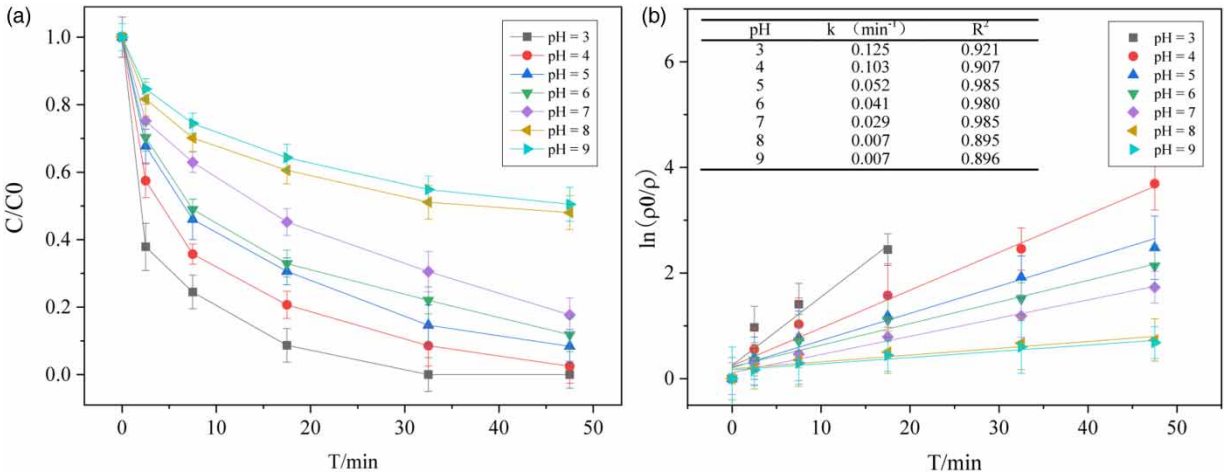

Figure 6 | (a) The degradation of oxytetracycline under different pH conditions, and (b) degradation kinetics of oxytetracycline under different pH conditions (initial OTC concentration = 50 mg L^{-1}, PDS concentration = 1 mM, [NGO-Fe_3O_4]:[PDS] = 4:1, pH = 3, 4, 5, 6, 7, 8, 9, temperature = 20 ± 2 °C, xenon lamp (500 W/50 Hz)).

Initial OTC concentration

OTC concentration was a vital factor for the degradation efficiency and the practical application of the process. Figure 7 shows the effect of different initial OTC concentrations on the degradation efficiency. The results showed that the OTC degradation efficiency was 100%, 97.01%, 83.01%, 59.01% and 42.84%, with initial OTC concentration of 20, 50, 100, 200 and 300 mg L^{-1}, respectively. The k_{obs} decreased from 0.112 min^{-1} to 0.008 min^{-1}. This can be explained by the following three reasons. Firstly, intermediates that accumulate rapidly during the reaction process compete with OTC in the system for a limited number of active substances, leading to a decrease in the OTC degradation efficiency. Secondly, while the concentration of OTC increased, the amount of OTC adsorbed on the surface of NGO-Fe_3O_4 increased, resulting in a decrease in the active site on the surface of NGO-Fe_3O_4. Finally, high OTC concentration increased the difficulty of light penetration, making it difficult for photons to reach and act on the catalyst, which evidently diminished the OTC degradation efficiency (Li *et al.* 2018).

Quenching experiments

Based on the abovementioned reactions (Equations (1) and (4)), both ·OH and SO_4^{-}· may be present in the Vis/NGO-Fe_3O_4/PDS system. To estimate their contribution to OTC

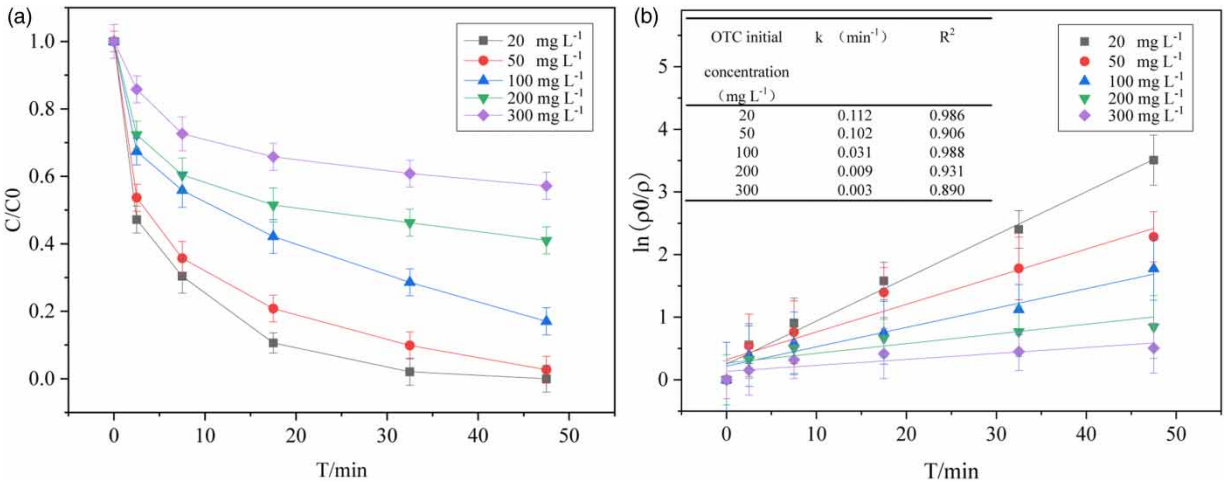

Figure 7 | (a) The degradation of oxytetracycline under different initial concentration, and (b) degradation kinetics of oxytetracycline under different initial concentration (initial OTC concentration = 20, 50, 100, 200, 300 mg L^{-1}, PDS concentration = 1 mM, [NGO-Fe_3O_4]:[PDS] = 4:1, pH = 3.0, temperature = 20 ± 2 °C, xenon lamp (500 W/50 Hz)).

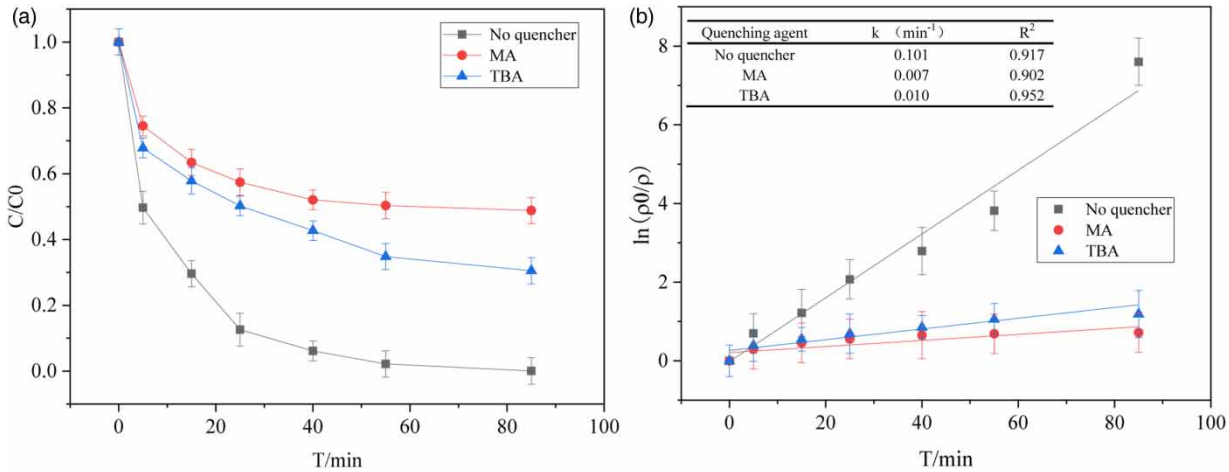

Figure 8 | (a) The degradation of oxytetracycline under different quencher conditions, and (b) degradation kinetics of oxytetracycline under different quencher (initial OTC concentration = 50 mg L^{-1}, PDS concentration = 1 mM, [NGO-Fe_3O_4]:[PDS] = 4:1, pH = 3.0, temperature = 20 ± 2 °C, xenon lamp (500 W/50 Hz)).

degradation in the Vis/NGO-Fe_3O_4/PDS system, methanol (MA, scavenger of both ·OH and SO_4^{-}·) and tert-butanol (TBA, scavenger of ·OH alone) were added to the reaction system at a ratio of 500:1 to PDS. As shown in Figure 8, the corresponding suppression ratios (k_{obs} OTC(Blank)/k_{obs} OTC(Scavenger)) were obtained as 14.4 and 10.1, respectively. MA could lead to a higher suppression ratio than TBA. ·OH would be the main but not the only reactive oxygen species for the OTC degradation, suggesting that SO_4^{-}· would also participate in oxidizing OTC.

Reusability of NGO-Fe_3O_4

In order to evaluate the stability of NGO-Fe_3O_4, NGO-Fe_3O_4 separated from the solution was washed three times with deionized water and reused in the next cycle. Five successive catalytic degradation experiments were carried out under the optimal conditions (i.e. PDS = 1 mM, [NGO-Fe_3O_4]:[PDS] = 4:1, pH = 3.0). Figure 9 shows that the OTC degradation was not significantly deteriorated after five successive cycles.

Analysis of OTC degradation pathways

The intermediate products of OTC degradation by Vis/NGO-Fe_3O_4/PDS system under optimal condition (i.e. PDS = 1 mM, [NGO-Fe_3O_4]:[PDS] = 4:1, pH = 3.0) were detected by LC-MS. The molecular formula and molecular structures are listed in Table 1 and the OTC degradation pathway is proposed. Generally, as an electrophilic agent, SO_4^{-}· had a similar reaction mechanism to that of ·OH,

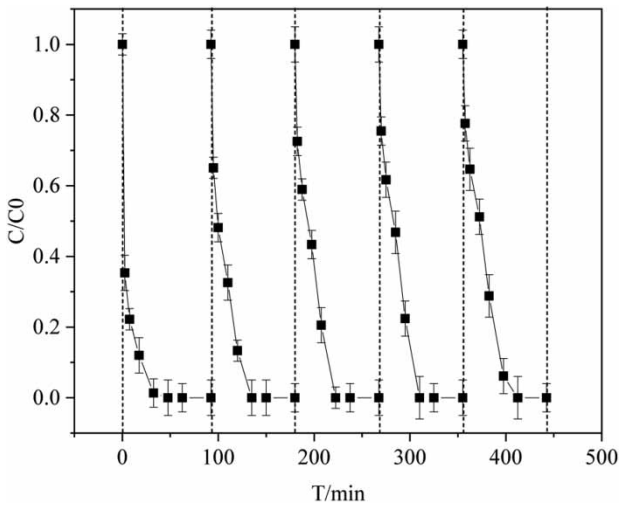

Figure 9 | Repeated degradation and recovery of oxytetracycline by Vis/NGO-Fe_3O_4/PDS (initial OTC concentration = 50 mg L^{-1}, PDS concentration = 1 mM, [NGO-Fe_3O_4]:[PDS] = 4:1, pH = 3.0, temperature = 20 ± 2 °C, xenon lamp (500 W/50 Hz)).

i.e., (1) hydrogen abstraction, (2) hydroxyl addition to unsaturated carbon, and (3) more significant electronic transfer (He *et al.* 2014; Khan *et al.* 2014). The aromatic ring (such as ring D, in Figure 10), C_{11}=C_{12} and C_1=C_3 keto/enol moieties, hydroxyl group at C_5 and dimethylammonium group at C_4 in the OTC structure were potential targets for SO_4^{-}· attack (Liu *et al.* 2016a). Due to the low bond energy of N-C and C-O in the OTC structure, the living radicals can react with the OTC and cause the loss of N-methyl, amino, carbonyl, formyl and hydroxyl groups, and finally OTC is turned into intermediates with a similar structure (Chen *et al.* 2016).

Table 1 | The intermediate products in the oxytetracycline degradation

Product	m/z detection value	Possible structural formula	Molecular formula	Molecular weight
I	503.07	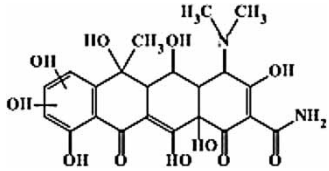	$C_{22}H_{24}N_2O_{11}$	493
II(1)		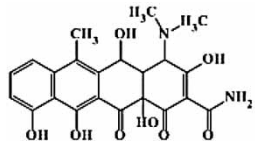	$C_{22}H_{22}N_2O_8$	443
II(2)	459.08	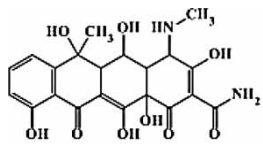	$C_{21}H_{22}N_2O_9$	447
II(3)		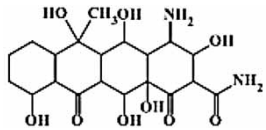	$C_{20}H_{30}N_2O_9$	442
III(1)		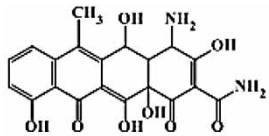	$C_{20}H_{18}N_2O_8$	414
III(2)	415.09	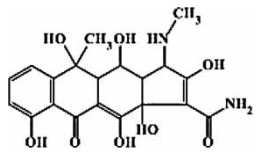	$C_{20}H_{22}N_2O_8$	418
III(3)		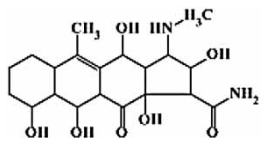	$C_{20}H_{30}N_2O_7$	410
IV	329.12	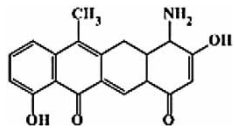	$C_{19}H_{17}NO_4$	323
V	263.14	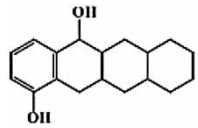	$C_{18}H_{24}O_2$	272
VI	113.04	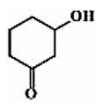	$C_6H_{10}O_2$	114

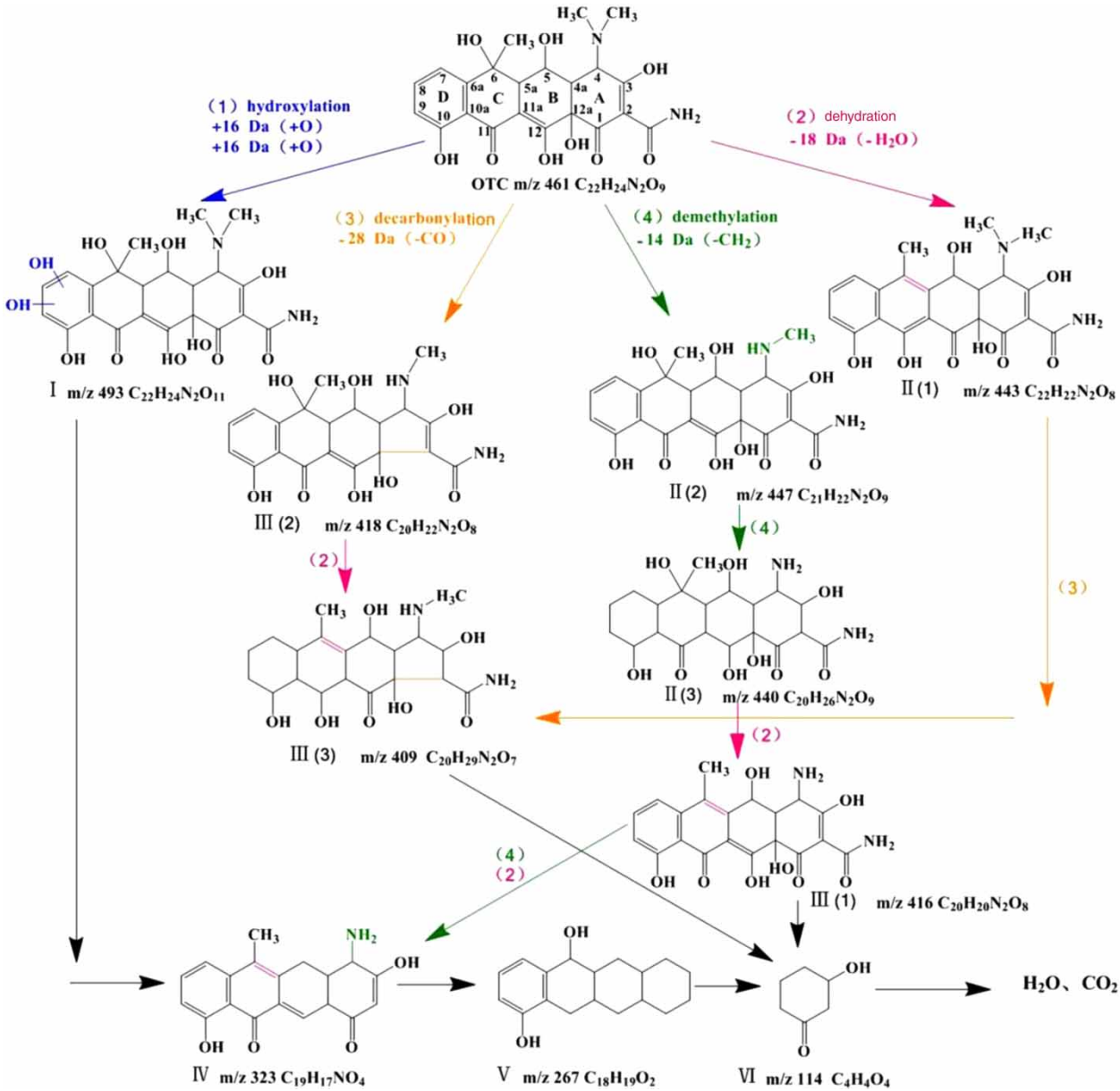

Figure 10 | The chemical structure and proposed degradation pathway of oxytetracycline.

According to the above discussion, four degradation pathways were proposed, namely hydroxylation, dehydration, decarbonylation and demethylation. Hydroxylation (pathway (1)) was a significant reaction of the OTC degradation process in the Vis/NGO-Fe_3O_4/PDS reaction system. It seemed that OTC was hydroxylated by adding unsaturated carbon or hydrogen abstraction on the saturated carbon of the hydroxyl or amino group to obtain product I (Table 1) (Ji *et al.* 2016). The dehydration reaction pathway (pathway (2)) can occur at C_5, C_6 or C_{12a}. The dehydration at C_6 could lead to the formation of a stable second aromatic C ring making it to be a more likely reaction site, resulting in the formation of a stable aromatic ring (product II(1)) at C based on the tautomerization of the C_{11}–C_{12} keto/enol (Liu *et al.* 2016b). Decarbonylation (pathway (3)) was the reaction to a loss of =CO on the ring structure (Liu *et al.* 2016a). The decarbonylation byproduct m/z 418 (product III(2)) would more likely be a diradical intermediate produced by the cleavage of C_1–C_{12a} in $SO_4^{\cdot-}$ attacking OTC. Demethylation (pathway (4)) refers to the removal of one methyl group from the dimethylammonium group at C_4 resulting in the generation of the byproduct m/z 447 (product II(2)). Liu *et al.* (2016b)

pointed out that $SO_4^{\cdot-}$ could induce the demethylation reaction starting with hydrogen abstraction at the methyl moiety. The methyl group on the nitrogen atom in product II(2) was further substituted with a hydrogen radical to generate product II(3).

CONCLUSION

A high OTC removal efficiency could be reached within 32.5 min by the Vis/NGO-Fe_3O_4/PDS system, indicating a significant synergistic effect. The degradation constants followed the first-order kinetics. Four degradation pathways (hydroxylation, dehydration, decarbonylation and demethylation) were proposed. The Vis/NGO-Fe_3O_4/PDS system can maintain high OTC degradation efficiency over a wide pH range. Moreover, NGO-Fe_3O_4 exhibited excellent stability in repeated recycling experiments. This study has revealed a distinguished homogeneous–heterogeneous reaction system for the degradation of recalcitrant pollutants.

ACKNOWLEDGEMENTS

The authors acknowledge Henan Provincial Department of Science and Technology Research Project (172102310562).

REFERENCES

Bi, W., Wu, Y., Wang, X., Zhai, P. & Dong, W. 2016 Degradation of oxytetracycline with $SO_4^{\cdot-}$ under simulated solar light. *Chem. Eng. J.* **302**, 811–818.

Chen, M. & Chu, W. 2012 Degradation of antibiotic norfloxacin in aqueous solution by visible-light-mediated C-TiO_2 photocatalysis. *J. Hazard. Mater.* **219–220**, 183–189.

Chen, C. & Zheng, Y. 2015 Degradation of oxytetracycline in wastewater by multi-frequency ultrasonic. *Chem. Ind. Eng. Prog.* **34**, 1143–1146.

Chen, H., Peng, Y., Chen, K., Lai, C. & Lin, Y. 2016 Rapid synthesis of Ti-MCM-41 by microwave-assisted hydrothermal method towards photocatalytic degradation of oxytetracycline. *J. Environ. Sci.* **44**, 76–87.

Christgau, S., Henrotin, Y., Tankó, L. B., Rovati, L. C., Collette, J., Bruyere, O., Deroisy, R. & Reginster, J. Y. 2004 Osteoarthritic patients with high cartilage turnover show increased responsiveness to the cartilage protecting effects of glucosamine sulphate. *Clin. Exp. Rheumatol.* **22**, 36.

Criquet, J. & Leitner, N. K. 2009 Degradation of acetic acid with sulfate radical generated by persulfate ions photolysis. *Chemosphere* **77**, 194–200.

Ding, D., Liu, C., Ji, Y., Yang, Q., Chen, L., Jiang, C. & Cai, T. 2017 Mechanism insight of degradation of norfloxacin by magnetite nanoparticles activated persulfate: identification of radicals and degradation pathway. *Chem. Eng. J.* **308**, 330–339.

Donghui, L., Wei, L., Licheng, L., Jin, M., Isao, M. & Seong-Ho, Y. 2010 Preparation of nitrogen-doped graphene sheets by a combined chemical and hydrothermal reduction of graphene oxide. *Langmuir* **26**, 16096–16102.

Duan, X., Sun, H., Tade, M. & Wang, S. 2017 Metal-free activation of persulfate by cubic mesoporous carbons for catalytic oxidation via radical and nonradical processes. *Catal. Today* **307**, 140–146.

Figueroa, R. A., Leonard, A. & Mackay, A. A. 2004 Modeling tetracycline antibiotic sorption to clays. *Environ. Sci. Technol.* **38**, 476–483.

He, X., Aa, D. L. C., O'Shea, K. E. & Dionysiou, D. D. 2014 Kinetics and mechanisms of cylindrospermopsin destruction by sulfate radical-based advanced oxidation processes. *Water Res.* **63**, 168–178.

Hu, X. B., Deng, Y. H., Gao, Z. Q., Liu, B. Z. & Cheng, S. 2012 Transformation and reduction of androgenic activity of 17α-methyltestosterone in Fe_3O_4/MWCNTs–H_2O_2 system. *App. Catal. B. Environ.* **127**, 167–174.

Huang, L., Man, W., Shi, C., Ji, H. & Bo, Z. 2014 Adsorption of tetracycline and ciprofloxacin on activated carbon prepared from lignin with H_3PO_4 activation. *Desalin. Water Treat.* **52**, 2678–2687.

Ji, Y., Shi, Y., Wei, D., Xin, W., Jiang, M. & Lu, J. 2016 Thermo-activated persulfate oxidation system for tetracycline antibiotics degradation in aqueous solution. *Chem. Eng. J.* **298**, 225–233.

Khan, J. A., He, X., Shah, N. S., Khan, H. M., Hapeshi, E., Fatta-Kassinos, D. & Dionysiou, D. D. 2014 Kinetic and mechanism investigation on the photochemical degradation of atrazine with activated H_2O_2, $S_2O_8^{2-}$ and HSO_5^-. *Chem. Eng. J.* **252**, 393–403.

Lai, L., Chen, L., Zhan, D., Sun, L., Liu, J., Lim, S. H., Poh, C. K., Shen, Z. & Lin, J. 2011 One-step synthesis of NH_2-graphene from in situ graphene-oxide reduction and its improved electrochemical properties. *Carbon* **49**, 3250–3257.

Li, B., Lai, C., Zeng, G., Qin, L., Yi, H., Huang, D., Zhou, C., Liu, X., Cheng, M. & Xu, P. 2018 Facile hydrothermal synthesis of Z-scheme $Bi_2Fe_4O_9$/Bi_2WO_6 heterojunction photocatalyst with enhanced visible light photocatalytic activity. *ACS Appl. Mater. Interfaces* **10**, 18824–18836.

Liu, Y., He, X., Fu, Y. & Dionysiou, D. D. 2016a Kinetics and mechanism investigation on the destruction of oxytetracycline by UV-254 nm activation of persulfate. *J. Hazard Mater* **305**, 229–239.

Liu, Y., He, X., Fu, Y. & Dionysiou, D. D. 2016b Degradation kinetics and mechanism of oxytetracycline by hydroxyl radical-based advanced oxidation processes. *Chem. Eng. J.* **284**, 1317–1327.

Liu, C., Li, X., Li, J., Zhou, Y., Sun, L., Wang, H., Huo, P., Ma, C. & Yan, Y. 2019 Fabricated 2D/2D CdIn 2 S 4/N-rGO muti-heterostructure photocatalyst for enhanced photocatalytic activity. *Carbon* **152**, 565–574.

Luu, H. T. & Lee, K. 2014 Degradation and changes in toxicity and biodegradability of tetracycline during ozone/ultraviolet-based advanced oxidation. *Water Sci. Technol.* **70**, 1229–1235.

Olmezhanci, T., Arslanalaton, I. & Genc, B. 2013 Bisphenol A treatment by the hot persulfate process: oxidation products and acute toxicity. *J. Hazard. Mater* **263**, 283–290.

Oturan, N., Wu, J., Zhang, H., Sharma, V. K. & Oturan, M. A. 2013 Electrocatalytic destruction of the antibiotic tetracycline in aqueous medium by electrochemical advanced oxidation processes: effect of electrode materials. *Appl. Catal. B Environ.* **140–141**, 92–97.

Peng, G., Zhang, M., Deng, S., Shan, D., Qiang, H. & Gang, Y. 2018 Adsorption and catalytic oxidation of pharmaceuticals by nitrogen-doped reduced graphene oxide/Fe_3O_4 nanocomposite. *Chem. Eng. J.* **341**, 361–370.

Pereira, J. H. O. S., Vilar, V. J. P., Borges, M. T., González, O., Esplugas, S. & Rui, A. R. B. 2011 Photocatalytic degradation of oxytetracycline using TiO under natural and simulated solar radiation. *Sol. Energy.* **85**, 2732–2740.

Pu, M., Guan, Z., Ma, Y., Wan, J., Wang, Y., Brusseau, M. L. & Chi, H. 2017 Synthesis of iron-based metal-organic framework MIL-53 as an efficient catalyst to activate persulfate for the degradation of Orange G in aqueous solution. *Appl. Catal. A Gen.* **549**, 82–92.

Sharma, V., Kumar, R. V., Pakshirajan, K. & Pugazhenthi, G. 2017 Integrated adsorption-membrane filtration process for antibiotic removal from aqueous solution. *Powder Technol.* **321**, 259–269.

Shiraz A, D., Takdastan, A. & Borghei, S. M. 2017 Photo-Fenton like degradation of catechol using persulfate activated by UV and ferrous ions: influencing operational parameters and feasibility studies. *J. Mol. Liq.* **249**, 463–469.

Wang, X., Qin, Y., Zhu, L. & Tang, H. 2015 Nitrogen-doped reduced graphene oxide as a bifunctional material for removing bisphenols: synergistic effect between adsorption and catalysis. *Environ. Sci. Technol.* **49**, 6855–6864.

Wang, Y., Jia, H., Zhang, H., Wang, J. & Liu, W. 2017 Performance of a novel recycling magnetic flocculation membrane filtration process for tetracycline-polluted surface water treatment. *Water Sci. Technol.* **33**, 490–500.

Watkinson, A. J., Murby, E. J. & Costanzo, S. D. 2007 Removal of antibiotics in conventional and advanced wastewater treatment: implications for environmental discharge and wastewater recycling. *Water Res.* **41**, 4164–4176.

Watkinson, A. J., Murby, E. J., Kolpin, D. W. & Costanzo, S. D. 2009 The occurrence of antibiotics in an urban watershed: from wastewater to drinking water. *Sci. Total Environ.* **407**, 2711–2723.

Xinran, W., Xiaolin, L., Li, Z., Youngki, Y., Weber, P. K., Hailiang, W., Jing, G. & Hongjie, D. 2009 N-doping of graphene through electrothermal reactions with ammonia. *Science* **324**, 768–771.

Xiong, X., Sun, B., Zhang, J., Gao, N., Shen, J., Li, J. & Guan, X. 2014 Activating persulfate by Fe^0 coupling with weak magnetic field: performance and mechanism. *Water Res.* **62**, 53–62.

Zhen, M., Guo, S., Gao, G., Zhou, Z. & Liu, L. 2014 TiO_2-B nanorods on reduced graphene oxide as anode materials for Li ion batteries. *Chem. Commun.* **51**, 507–510.

Zhu, H. 2019 Fe_3O_4/granular activated carbon as an efficient three-dimensional electrode to enhance the microbial electrosynthesis of acetate from CO_2. *RSC Adv.* **9**, 34095–34101.

Zhu, X., Liu, Y., Zhou, C., Luo, G., Zhang, S. & Chen, J. 2014 A novel porous carbon derived from hydrothermal carbon for efficient adsorption of tetracycline. *Carbon* **77**, 627–636.

First received 14 January 2020; accepted in revised form 27 March 2020. Available online 7 April 2020